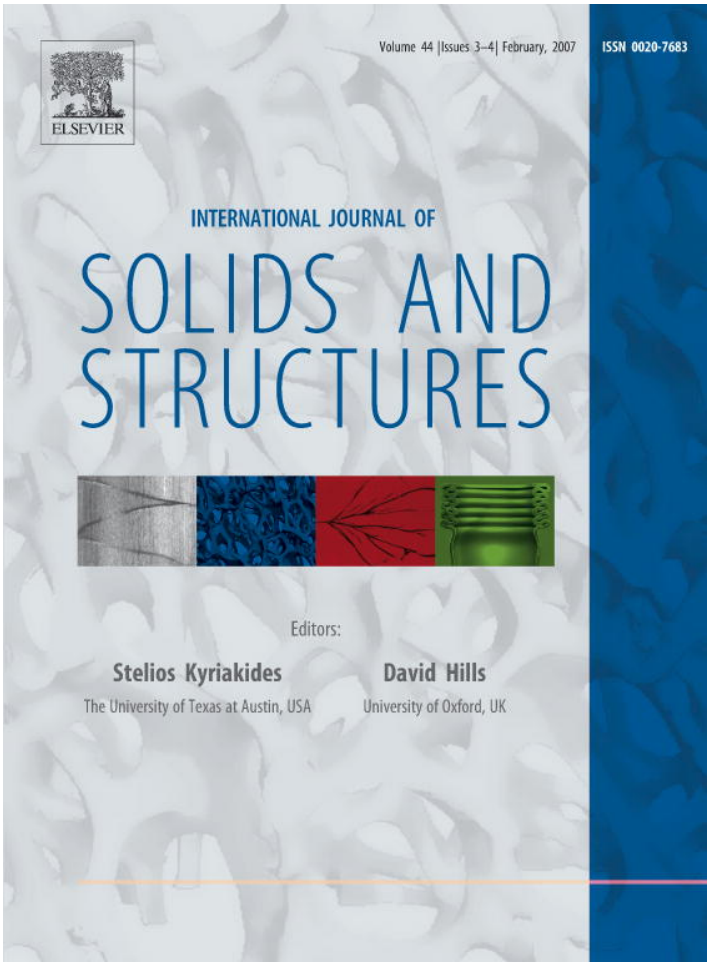

Available online at www.sciencedirect.com
ScienceDirect
International Journal of Solids and Structures 44 (2007) 1073–1085
INTERNATIONAL JOURNAL OF SOLIDS and STRUCTURES
www.elsevier.com/locate/ijsolstr

Wave propagation in magneto-electro-elastic multilayered plates

Jiangyi Chen [a], E. Pan [b,*], Hualing Chen [a]

[a] School of Mechanical Engineering, Xi'an Jiaotong University, 710049 Xi'an, PR China
[b] Department of Civil Engineering, The University of Akron, ASEC, Akron, OH 44325-3905, USA

Received 21 September 2005; received in revised form 24 May 2006
Available online 10 June 2006

Abstract

An analytical treatment is presented for the propagation of harmonic waves in magneto-electro-elastic multilayered plates, where the general anisotropic and three-phase coupled constitutive equations are used. The state-vector approach is employed to derive the propagator matrix which connects the field variables at the upper interface to those at the lower interface of each layer. The global propagator matrix is obtained by propagating the solution in each layer from the bottom of the layered plate to the top using the continuity conditions of the field variables across the interfaces. From the global propagator matrix, we finally obtain the dispersion relation by imposing the traction-free boundary condition on the top and bottom surfaces of the layered plate. Dispersion curves, modal shapes, and natural frequencies are presented for layered plates made of orthotropic elastic (graphite–epoxy), transversely isotropic PZT-5A, piezoelectric $BaTiO_3$ and magnetostrictive $CoFe_2O_4$ materials. While the numerical results show clearly the influence of different stacking sequences as well as material properties on the field response, the general methodology presented in the paper could be useful to the analysis and design of layered composites made of smart piezoelectric and piezomagnetic materials.

Keywords: Piezoelectricity; Magnetostrictive material; Anisotropy; State-vector approach; Propagator matrix; Dispersion curve; Modal shape; Wave propagation; Natural frequency

1. Introduction

In recent years, composites made of piezoelectric and/or piezomagnetic phases have been increasingly applied to different engineering structures, especially to the smart or intelligent systems as intelligent sensors, damage detectors, etc. (Achenbach, 2000; Buchanan, 2003). These composites possess certain new product properties (e.g. the magneto-electric effect), which are not demonstrated with their individual components. Various analytical/numerical studies have been carried out for these multiphase and multifunctional materials. These include studies on the static deformation (Pan, 2001), free vibration (Pan and Heyliger,

* Corresponding author. Tel.: +1 3309726739; fax: +1 3309726020.
E-mail address: pan2@uakron.edu (E. Pan).

0020-7683/$ - see front matter © 2006 Elsevier Ltd. All rights reserved.
doi:10.1016/j.ijsolstr.2006.06.003

2002; Chen et al., 2005, in press), and on the effective bulk material properties (Shin et al., 1998; Chen et al., 2002).

For a homogeneous plate made of either isotropic or anisotropic material, the dispersion relation for guided waves was studied several decades ago (Achenbach, 1973; Graff, 1975). For instance, for a bilayered isotropic plate, Jones (1964) studied the phase velocity vs. wavenumber behavior when the top layer has different thicknesses. Safaeinili et al. (1995) discussed the Floquet wave propagation in periodically layered composites. There are also many articles on wave propagation in layered structures with particular emphasis on the NDE application (Fahmy and Adler, 1973; Chimenti, 1997; Pan et al., 1999). More recently, wave problems in piezoelectric and piezomagnetic structures are widely investigated, with literature being mostly focused on the piezoelectric materials (Minagawa, 1995; Faidi and Nayfeh, 2000; Liu et al., 2001, 2003; Wang and Varadan, 2002).

In terms of methodology for solving problems in layered systems, the propagator matrix and the state-vector (or state space) approaches are the most popular methods among others (e.g., Thomson, 1950; Haskell, 1953; Gilbert and Backus, 1966; Bahar, 1975). Due to their conceptual simplicity and reduced programming effort and computing time, these approaches have now been extended to various complicated layered structures, including, for example, static and free vibration analysis of piezoelectric or magneto-electro-elastic plates (Lee and Jiang, 1996; Wang et al., 2003; Chen et al., in press), derivation of Green's functions (Pan, 1997), wave propagation in purely elastic and piezoelectric layered structures (Fahmy and Adler, 1973; Wang and Rokhlin, 2002, 2004). To the best of the authors' knowledge, however, wave propagation in magneto-electro-elastic multilayered plates has not been investigated so far, which is the motivation of this study.

In this paper, an analytical treatment on the propagation of harmonic waves in an infinitely extended, magneto-electro-elastic, and multilayered plate is presented. The constitutive relation used is of general anisotropy with piezoelectric and piezomagnetic coupling. By virtue of the state-vector approach, the general displacements and stresses of the medium are divided into the so-called 'out-of-plane variables' and 'in-plane variables'. The propagator matrix, which connects the 'out-of-plane variables' at the top and bottom interface of each layer, is derived by solving the state-vector equation. Then the propagator matrix is propagated from one layer to the other using the continuity condition at the interface of the layers. Making use of the general traction-free boundary conditions on the top and bottom surfaces of the layered plate, a simple dispersion equation is obtained from the final propagator matrix. Numerical examples are also presented to show the features of the dispersion curves as well as the corresponding modal shapes, which should be of interest to the future modeling and simulation using numerical methods.

This paper is organized as follows: In Section 2, we present the basic equations in terms of the state-vector approach. In Section 3, we derive the dispersion relation for the layered plate. While numerical examples are given in Section 4, conclusions are drawn in Section 5.

2. Governing equations

Consider an anisotropic, magneto-electro-elastic, and N-layered plate which is infinite horizontally but finite in the vertical (thickness) direction with a total thickness H. We place the horizontal (x,y)-plane of a Cartesian coordinate system on the bottom surface and let the plate be in the positive z-region. Layer j is bonded by the lower interface z_j and upper interface z_{j+1} with thickness $h_j = z_{j+1} - z_j$ $(j = 1,2,\ldots,N)$. We assume that the general displacement and traction vectors are continuous across the interface, and that on the top and bottom surfaces of the plate, the general traction vector is zero.

For a linear, anisotropic, and magneto-electro-elastic solid, the coupled constitutive equation can be written in the following form

$$\sigma_i = c_{ik}\gamma_k - e_{ki}E_k - q_{ki}H_k, \quad D_i = e_{ik}\gamma_k + \varepsilon_{ik}E_k + d_{ik}H_k, \quad B_i = q_{ik}\gamma_k + d_{ik}E_k + \mu_{ik}H_k \tag{1}$$

where σ_i, D_i and B_i are the stress, electric displacement, and magnetic induction, respectively; γ_k, E_k and H_k are the strain, electric field, and magnetic field, respectively; c_{ik}, e_{ik} and q_{ik} are the 6×6 elastic, 3×6 piezoelectric, and 3×6 piezomagnetic coefficient matrices, respectively; ε_{ik}, d_{ik}, and μ_{ik} are the 3×3 dielectric, magnetic permeability, and magneto-electric coefficients, respectively. We mention that various uncoupled cases can be reduced by setting the appropriate coupling coefficients to zero.

The relationship between the general strain and general displacement can be expressed as

$$\gamma_{ij} = 0.5(u_{i,j} + u_{j,i}), \quad E_i = -\varphi_{,i}, \quad H_i = -\psi_{,i} \tag{2}$$

where

$$u_i = [u \quad v \quad w]^{\mathrm{T}} \tag{3}$$

are the elastic displacements, φ and ψ are the electric potential and magnetic potential respectively.

For the wave propagation considered in this paper, the body forces, electric charge and current density are assumed to be zero. Thus, the dynamic equation for the magneto-electro-elastic plate is governed by

$$\sigma_{ij,j} = \rho \frac{\partial^2 u_i}{\partial t^2}, \quad D_{j,j} = 0, \quad B_{j,j} = 0 \tag{4}$$

with ρ being the density of the material. Eqs. (1) and (4) contain 17 equations and 17 unknowns. The 17 unknowns are: three elastic displacements, six stresses, three electric displacements and magnetic inductions, one electric potential and magnetic potential. Therefore, the 17 unknowns can be determined by solving the 17 equations (1)–(4).

Furthermore, the 17 unknowns can be divided into two categories: One is called the 'out-of-plane variables' (related to the general displacement and traction which are taken as the primary variables); the other is called the 'in-plane variables' (related to the in-plane stress, electrical displacement and magnetic displacement which are taken as the secondary variables). The primary variables are expressed by the vector form

$$\boldsymbol{\eta} = [u \quad v \quad D_z \quad B_z \quad \sigma_z \quad \tau_{zx} \quad \tau_{zy} \quad \varphi \quad \psi \quad w]^{\mathrm{T}} \tag{5}$$

where the subscripts x, y and z correspond to subscripts 1, 2 and 3 in Eqs. (1), (2) and (4). With the state-vector approach, the secondary variables can be determined through the primary variables. However, for simplicity, only the state-vector equation for the primary variables is derived, which can be written as

$$\frac{\partial \boldsymbol{\eta}}{\partial z} = \boldsymbol{A}\boldsymbol{\eta} \tag{6}$$

where, for the 6 mm crystal material, the matrix $\boldsymbol{A}$ is given by

$$\boldsymbol{A} = \begin{bmatrix} 0 & \boldsymbol{A}_1 \\ \boldsymbol{A}_2 & 0 \end{bmatrix} \tag{7}$$

and

$$\boldsymbol{A}_1 = \begin{bmatrix} \frac{1}{c_{55}} & 0 & -\frac{e_{15}}{c_{55}}\frac{\partial}{\partial x} & -\frac{q_{15}}{c_{55}}\frac{\partial}{\partial x} & -\frac{\partial}{\partial x} \\ 0 & \frac{1}{c_{44}} & -\frac{e_{24}}{c_{44}}\frac{\partial}{\partial y} & -\frac{q_{24}}{c_{44}}\frac{\partial}{\partial y} & -\frac{\partial}{\partial y} \\ & & \left(\varepsilon_{11} + \frac{e_{15}^2}{c_{55}}\right)\frac{\partial^2}{\partial x^2} + \left(\varepsilon_{22} + \frac{e_{24}^2}{c_{44}}\right)\frac{\partial^2}{\partial y^2} & \left(d_{11} + \frac{e_{15}q_{15}}{c_{55}}\right)\frac{\partial^2}{\partial x^2} + \left(d_{22} + \frac{e_{24}q_{24}}{c_{44}}\right)\frac{\partial^2}{\partial y^2} & 0 \\ & & \textbf{Sym} & \left(\mu_{11} + \frac{q_{15}^2}{c_{55}}\right)\frac{\partial^2}{\partial x^2} + \left(\mu_{22} + \frac{q_{24}^2}{c_{44}}\right)\frac{\partial^2}{\partial y^2} & 0 \\ & & & & \rho\frac{\partial^2}{\partial t^2} \end{bmatrix} \tag{8}$$

$$\boldsymbol{A}_2 = \begin{bmatrix} -\alpha_{11}\frac{\partial^2}{\partial x^2} - c_{66}\frac{\partial^2}{\partial y^2} + \rho\frac{\partial^2}{\partial t^2} & -\alpha_{12}\frac{\partial^2}{\partial x \partial y} - c_{66}\frac{\partial^2}{\partial x \partial y} & -v_{21}\frac{\partial}{\partial x} & -v_{31}\frac{\partial}{\partial x} & -v_{11}\frac{\partial}{\partial x} \\ & -\alpha_{22}\frac{\partial^2}{\partial y^2} - c_{66}\frac{\partial^2}{\partial x^2} + \rho\frac{\partial^2}{\partial t^2} & -v_{22}\frac{\partial}{\partial y} & -v_{32}\frac{\partial}{\partial y} & -v_{12}\frac{\partial}{\partial y} \\ & & \zeta_{22} & \zeta_{23} & \zeta_{12} \\ & \textbf{Sym} & & \zeta_{33} & \zeta_{13} \\ & & & & \zeta_{11} \end{bmatrix} \tag{9}$$

In Eq. (9),

$$\alpha_{ij} = c_{ij} - c_{i3}v_{1j} - e_{3i}v_{2j} - q_{3i}v_{3j} \quad (i = 1,2;\ j = 1,2) \tag{10}$$

$$v_{ij} = \zeta_{i1}c_{j3} + \zeta_{i2}e_{3j} + \zeta_{i3}q_{3j} \quad (i = 1,2,3;\ j = 1,2) \tag{11}$$

$$\zeta_{ij} = \xi_{ij}/\det\boldsymbol{\kappa} \quad (i = 1,2,3;\ j = 1,2,3) \tag{12}$$

with

$$\boldsymbol{\kappa} = \begin{bmatrix} c_{33} & e_{33} & q_{33} \\ e_{33} & -\varepsilon_{33} & -d_{33} \\ q_{33} & -d_{33} & -\mu_{33} \end{bmatrix} \tag{13}$$

and ξ_{ij} being the corresponding algebraic cofactors of $\boldsymbol{\kappa}$.

3. Dispersion relation

Considering a harmonic wave propagating along the azimuthal angle α measured from the positive x-axis in the anti-clockwise direction, the solution of Eq. (6) then can be assumed in the following form

$$\boldsymbol{\eta} = \tilde{\boldsymbol{\eta}}(z)\mathrm{e}^{\mathrm{i}(k_1x+k_2y-\omega t)} \tag{14}$$

where ω is the angular frequency, t the time, $\mathrm{i} = \sqrt{-1}$, and k_1, k_2 are the two components of the wave vector which are given by

$$k_1 = k\cos\alpha, \qquad k_2 = k\sin\alpha \tag{15}$$

with k being the magnitude of the wavenumber in the propagation direction. Also in Eq. (14), $\tilde{\boldsymbol{\eta}}(z)$ has been taken as

$$\tilde{\boldsymbol{\eta}}(z) = \begin{bmatrix} \tilde{u} & \tilde{v} & \mathrm{i}\tilde{D}_z & \mathrm{i}\tilde{B}_z & \mathrm{i}\tilde{\sigma}_z & \tilde{\tau}_{zx} & \tilde{\tau}_{zy} & \mathrm{i}\tilde{\varphi} & \mathrm{i}\tilde{\psi} & \mathrm{i}\tilde{w} \end{bmatrix}^{\mathrm{T}} \tag{16}$$

so that the elements of the matrix $\widetilde{\boldsymbol{A}}$ in Eq. (18) below are all real. Substituting Eq. (14) into Eq. (6) leads to

$$\frac{\mathrm{d}\tilde{\boldsymbol{\eta}}(z)}{\mathrm{d}z} = \widetilde{\boldsymbol{A}}(\omega,k)\tilde{\boldsymbol{\eta}}(z) \tag{17}$$

where

$$\widetilde{\boldsymbol{A}}(\omega,k) = \begin{bmatrix} 0 & \widetilde{\boldsymbol{A}}_1(\omega,k) \\ \widetilde{\boldsymbol{A}}_2(\omega,k) & 0 \end{bmatrix} \tag{18}$$

with

$$\widetilde{\boldsymbol{A}}_1(\omega,k) = \begin{bmatrix} \frac{1}{c_{55}} & 0 & -\frac{e_{15}}{c_{55}}k_1 & -\frac{q_{15}}{c_{55}}k_1 & -k_1 \\ 0 & \frac{1}{c_{44}} & -\frac{e_{24}}{c_{44}}k_2 & -\frac{q_{24}}{c_{44}}k_2 & -k_2 \\ \frac{e_{15}}{c_{55}}k_1 & \frac{e_{24}}{c_{44}}k_2 & -\left(\varepsilon_{11}+\frac{e_{15}^2}{c_{55}}\right)k_1^2-\left(\varepsilon_{22}+\frac{e_{24}^2}{c_{44}}\right)k_2^2 & -\left(d_{11}+\frac{e_{15}q_{15}}{c_{55}}\right)k_1^2-\left(d_{22}+\frac{e_{24}q_{24}}{c_{44}}\right)k_2^2 & 0 \\ \frac{q_{15}}{c_{55}}k_1 & \frac{q_{24}}{c_{44}}k_2 & -\left(d_{11}+\frac{e_{15}q_{15}}{c_{55}}\right)k_1^2-\left(d_{22}+\frac{e_{24}q_{24}}{c_{44}}\right)k_2^2 & -\left(\mu_{11}+\frac{q_{15}^2}{c_{55}}\right)k_1^2-\left(\mu_{22}+\frac{q_{24}^2}{c_{44}}\right)k_2^2 & 0 \\ k_1 & k_2 & 0 & 0 & -\rho\omega^2 \end{bmatrix} \tag{19}$$

$$\widetilde{\boldsymbol{A}}_2(\omega,k) = \begin{bmatrix} \alpha_{11}k_1^2+c_{66}k_2^2-\rho\omega^2 & (\alpha_{12}+c_{66})k_1k_2 & -v_{21}k_1 & -v_{31}k_1 & -v_{11}k_1 \\ (\alpha_{12}+c_{66})k_1k_2 & \alpha_{22}k_1^2+c_{66}k_2^2-\rho\omega^2 & -v_{22}k_2 & -v_{32}k_2 & -v_{12}k_2 \\ v_{21}k_1 & v_{22}k_2 & \zeta_{22} & \zeta_{32} & \zeta_{12} \\ v_{31}k_1 & v_{32}k_2 & \zeta_{32} & \zeta_{33} & \zeta_{13} \\ v_{11}k_1 & v_{12}k_2 & \zeta_{12} & \zeta_{13} & \zeta_{11} \end{bmatrix} \tag{20}$$

It is obvious that the general solution of Eq. (17) can be assumed as

$$\tilde{\boldsymbol{\eta}}(z) = \boldsymbol{B}\mathrm{e}^{\xi kz} \tag{21}$$

Substituting Eq. (21) into Eq. (17), we finally arrive at the following eigenvalue equation

$$[\widetilde{\boldsymbol{A}}(\omega, k) - \xi k\boldsymbol{I}]\boldsymbol{B} = 0 \tag{22}$$

Upon solving the eigenvalues and eigenvectors from Eq. (22), the general solution for the general displacement and traction vectors are derived as

$$\tilde{\boldsymbol{\eta}}(z) = \boldsymbol{\Psi}\langle \mathrm{e}^{\xi^* kz}\rangle \boldsymbol{K} \tag{23}$$

where $\boldsymbol{\Psi}$ is the eigenvector, $\langle \mathrm{e}^{\xi^* kz}\rangle$ is a diagonal matrix for the eigenvalues ξ^*, and $\boldsymbol{K}$ is a 10×1 column matrix to be determined. Let us assume that Eq. (23) is a general solution in the homogeneous layer j, with the top and bottom boundaries at h_j and 0 (locally), respectively. Let $z = 0$ in Eq. (23) and solve for the unknown constant column matrix, we find that

$$\boldsymbol{K} = \boldsymbol{\Psi}^{-1}\tilde{\boldsymbol{\eta}}(0) \tag{24}$$

Therefore, the solutions in the homogeneous layer j at any z can be expressed by those at $z = 0$ as

$$\tilde{\boldsymbol{\eta}}(z) = \boldsymbol{P}(z)\tilde{\boldsymbol{\eta}}(0) \tag{25}$$

where

$$\boldsymbol{P}(z) = \boldsymbol{\Psi}\langle \mathrm{e}^{\xi * kz}\rangle \boldsymbol{\Psi}^{-1} \tag{26}$$

is the propagator matrix, which relates to the z-coordinate only, and thus, holds in the global system as well. Therefore, relation (25) can be used repeatedly so that we can propagate the physical quantities from the bottom surface $z = 0$ to the top surface $z = H$ of the layered plate. Consequently, we have

$$\tilde{\boldsymbol{\eta}}(H) = \boldsymbol{P}_N(h_N)\boldsymbol{P}_{N-1}(h_{N-1})\cdots\boldsymbol{P}_1(h_1)\tilde{\boldsymbol{\eta}}(0) \tag{27}$$

where $h_j = z_{j+1} - z_j$ is the thickness of layer j and $\boldsymbol{P}_j$ again is the propagator matrix of layer j.

Eq. (27) is a surprising simple relation, and for given homogeneous boundary conditions, can be reduced to the dispersion equation, from which the natural frequencies of the system can be solved. As an example, we assume that the top and bottom surfaces are free boundaries (i.e., the elastic traction, the z-direction electric displacement, and magnetic induction are zero), we find that

$$\begin{bmatrix} \widetilde{\boldsymbol{S}}(H) \\ \boldsymbol{0} \end{bmatrix} = \begin{bmatrix} \boldsymbol{T}_{11} & \boldsymbol{T}_{12} \\ \boldsymbol{T}_{21} & \boldsymbol{T}_{22} \end{bmatrix} \begin{bmatrix} \widetilde{\boldsymbol{S}}(0) \\ \boldsymbol{0} \end{bmatrix} \tag{28}$$

where

$$\widetilde{\boldsymbol{S}} = \begin{bmatrix} \tilde{u} & \tilde{v} & \tilde{\phi} & \tilde{\psi} & \tilde{w} \end{bmatrix}^{\mathrm{T}} \tag{29}$$

and the submatrices $\boldsymbol{T}_{ij}$ are obtained from the multiplication of the propagator matrices in Eq. (27). Therefore, the dispersion relation is simply the condition that the determinant of the submatrix $\boldsymbol{T}_{21}$ vanishes, that is

$$\det[\boldsymbol{T}_{21}] = 0 \tag{30}$$

4. Numerical examples

In order to verify our approach, a purely elastic, 35-layered graphite–epoxy cross-ply laminated plate with 90°/0°/···/90°/0°/···/0°/90° configuration is considered (Karunasena et al., 1991). The top and bottom surfaces of the plate are traction-free and the material properties are given in Table 1.

Table 1
Elastic properties of 0° and 90° graphite/epoxy fibers (c_{ij} in 10^{11} N/m^2) from Karunasena et al. (1991)

Lamina	c_{11}	c_{33}	c_{13}	c_{55}
0°	1.6073	0.1392	0.0644	0.0707
90°	0.1392	0.1392	0.0692	0.0350

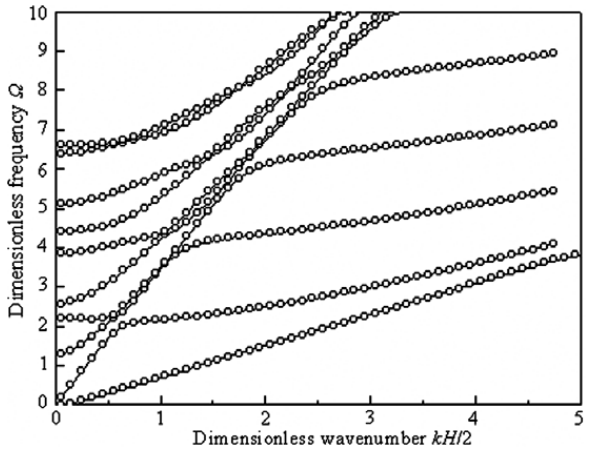

Fig. 1. Dispersion curves for the cross-ply graphite/epoxy plate with 35 layers.

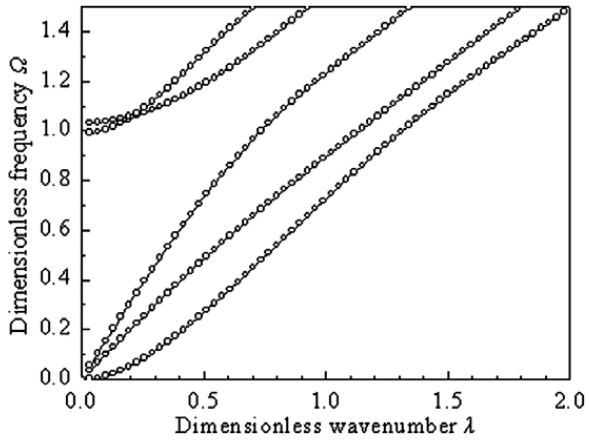

Fig. 2. Dispersion curves for the three-layer plate ZnO/ZnO/Si.

Fig. 1 shows the dispersion curve for the 35-layered laminated plate where the frequency and wavenumber are normalized as $\Omega = \frac{\omega H}{2\sqrt{(c_{55}/\rho)_0}}$ and $\lambda = kH/2$ with H being the total thickness of the plate. It is observed that Fig. 1 based on the present formulation is the same as Fig. 2(b) in Karunasena et al. (1991) for the normalized wavenumber varying from 0 to 5.

The second example for our verification is a three-layered piezoelectric plate, called "ZnO/ZnO/Si", where ZnO represents zinc oxide and Si the silicon with material properties being given in Stewart and Yong (1994). The thickness fractions for each layer are 0.36, 0.24 and 0.40 so that the total thickness is 1. Fig. 2 represents the dispersion relation for the three-layered plate under the open circuit condition with the normalization for the wavenumber and frequency being the same as in Stewart and Yong (1994). Again, it is observed that the present method (Fig. 2) predicts exactly the same dispersive curves as in the right half of Fig. 16 for the propagation modes in Stewart and Yong (1994).

Having verified our formulation for the purely elastic and piezoelectric multilayered plates, we now apply our solution to the three-layered plate composed of the magnetic and/or piezoelectric materials. Two cases are considered: One is a composite plate made of elastic graphite–epoxy and piezoelectric PZT-5A, and the other is the magneto-electro-elastic plate made of piezoelectric $BaTiO_3$ and magnetostrictive $CoFe_2O_4$. The three layers are assumed to have equal thickness, with material properties being listed in Table 2.

4.1. Three-layered graphite–epoxy/PZT-5A/graphite–epoxy plate

The first case considered is a three-layered composite plate with its top and bottom layers made of graphite–epoxy, and middle layer of PZT-5A. Fig. 3 shows the dispersion curves of the first seven modes for the wave

Table 2
Material properties (c_{ij} in 10^9 N/m^2, e_{ij} in C/m^2, q_{ij} in N/Am, ε_{ij} in 10^{-9} C^2/(N m^2), μ_{ij} in 10^{-6} N s^2/C^2, ρ in kg/m^3) from Ramirez et al. (2006)

Properties	$BaTiO_3$	$CoFe_2O_4$	PZT-5A	Graphite–epoxy	Properties	$BaTiO_3$	$CoFe_2O_4$	PZT-5A	Graphite–epoxy
c_{11}	166	286	99.201	183.443	$e_{31}=e_{32}$	−4.4	0	−7.209	0
c_{22}	166	286	99.201	11.662	e_{33}	18.6	0	15.118	0
c_{12}	77	173	54.016	4.363	$e_{24}=e_{15}$	11.6	0	12.322	0
c_{13}	78	170.5	50.778	4.363	$q_{31}=q_{32}$	0	580.3	0	0
c_{23}	78	170.5	50.778	3.918	q_{33}	0	699.7	0	0
c_{33}	162	269.5	86.856	11.662	$q_{24}=q_{15}$	0	550	0	0
c_{44}	43	45.3	21.1	2.87	$\varepsilon_{11}=\varepsilon_{22}$	11.2	0.08	1.53	1.53
c_{55}	43	45.3	21.1	7.17	ε_{33}	12.6	0.093	1.5	1.53
c_{66}	44.5	56.5	22.6	7.17	$\mu_{11}=\mu_{22}$	5	−590	5	5
ρ	5800	5300	7750	1590	μ_{33}	10	157	10	10

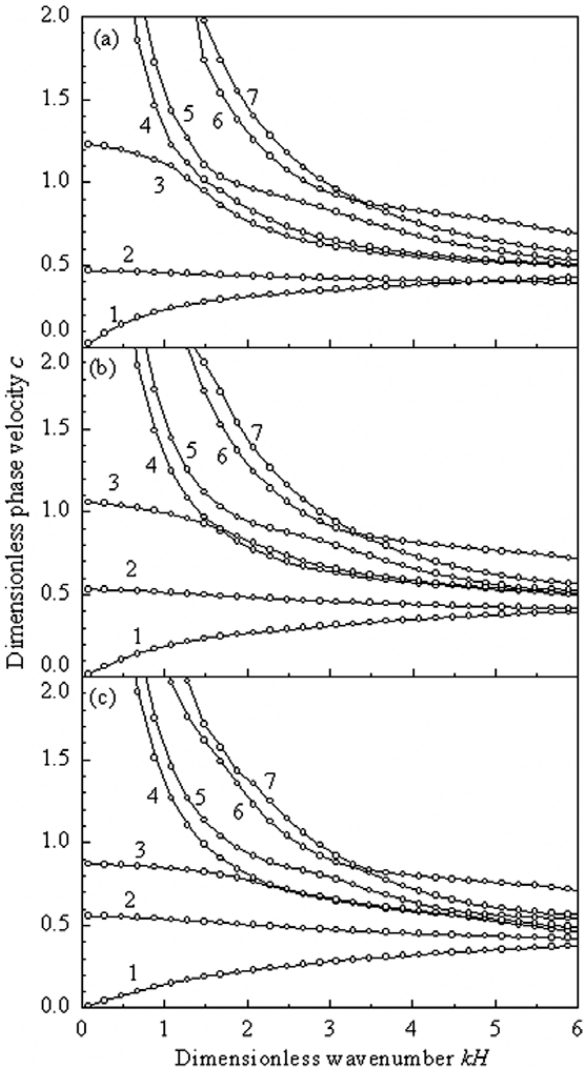

Fig. 3. Dispersion curves for the sandwich graphite–epoxy/PZT-5A/graphite–epoxy plate: (a) $\alpha = 30°$, (b) $\alpha = 45°$, and (c) $\alpha = 60°$.

propagating with different incident angles in the plate. The incident angles are 30°, 45° and 60° in Fig. 3(a)–(c), respectively. In these figures, while the horizontal axis is the dimensionless wavenumber kH, the vertical axis is the dimensionless phase velocity taken as $c = \frac{\omega}{k\sqrt{c_{\max}/\rho_{\max}}}$ with $c_{\max}$ being the maximum elastic stiffness element

of the layered plate and ρ_{max} the maximum density in the system. Comparing Fig. 3(a)–(c), we observe that the third mode significantly varies with the incident angle of the wave, in particular when the wavenumber is low. Actually, when the wavenumber is low (e.g., close to zero), its phase velocity on the third mode decreases with increasing incident angle (from 30° to 60°). On all other modes, on the other hand, the phase velocity curves are very similar to each other for different incident angles.

4.2. Three-layered plates made of $BaTiO_3$ and $CoFe_2O_4$

The three-layered plates with stacking sequences B/F/B, F/B/F, B/B/F, and F/F/B (B and F represent, respectively, $BaTiO_3$ and $CoFe_2O_4$) are investigated in this section. For comparison, results for the homogeneous plate made of piezoelectric $BaTiO_3$ (i.e., with a B/B/B stacking and is also called B only) and magnetostrictive $CoFe_2O_4$ (i.e., with an F/F/F stacking and is also called F only) are also presented. Due to the symmetry of transverse isotropy for these materials (with their symmetric axis being along the z-axis), an arbitrary incident angle can be chosen for the calculation of dispersion curves.

In Fig. 4(a)–(f), the dispersion curves for the first seven modes of the layered plate with the six different stacking sequences are presented. Comparing Fig. 4 to Fig. 3 and also Fig. 4(a)–(f) among themselves, one would notice that all these dispersion curves are very similar to each other. However, differences among them do exist if we present the dispersion curves for different stacking sequences in the same figure, as shown in

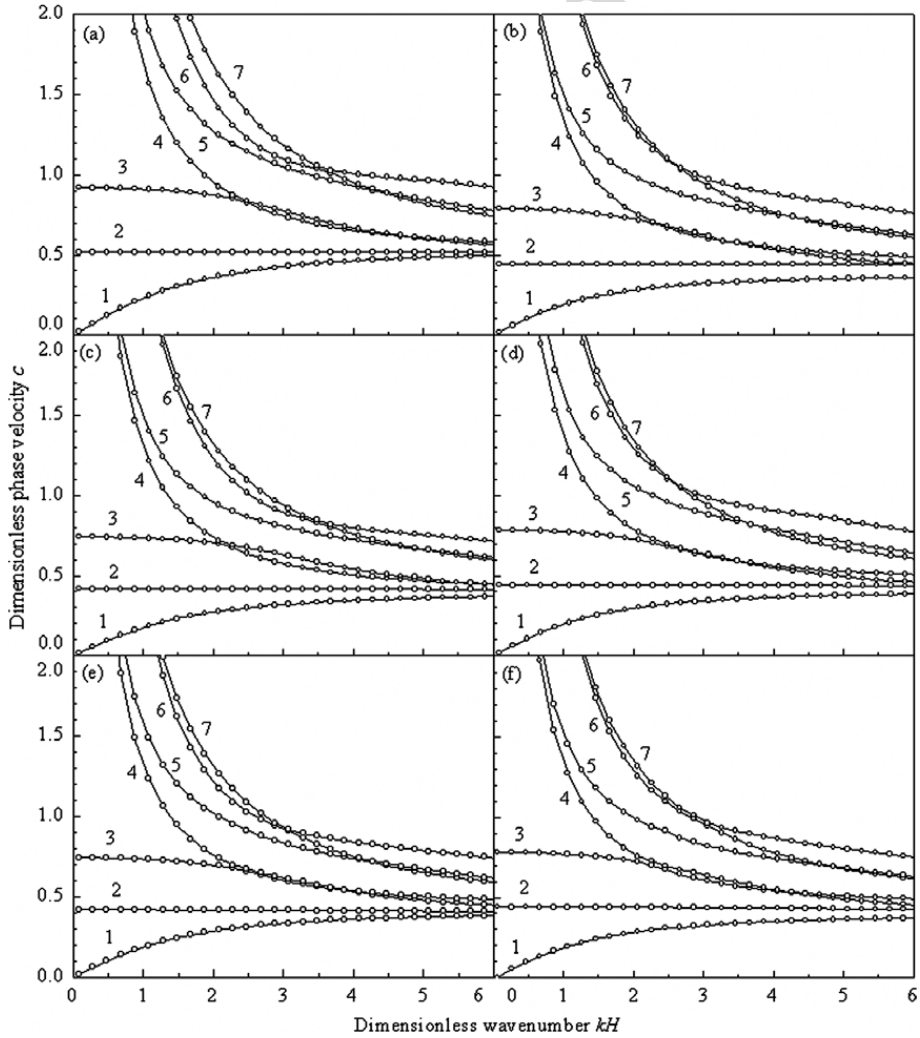

Fig. 4. Dispersion curves for the three-layered plate made of $BaTiO_3$ and $CoFe_2O_4$: (a) B only (B/B/B), (b) F only (F/F/F), (c) B/F/B, (d) F/B/F, (e) B/B/F, and (f) F/F/B.

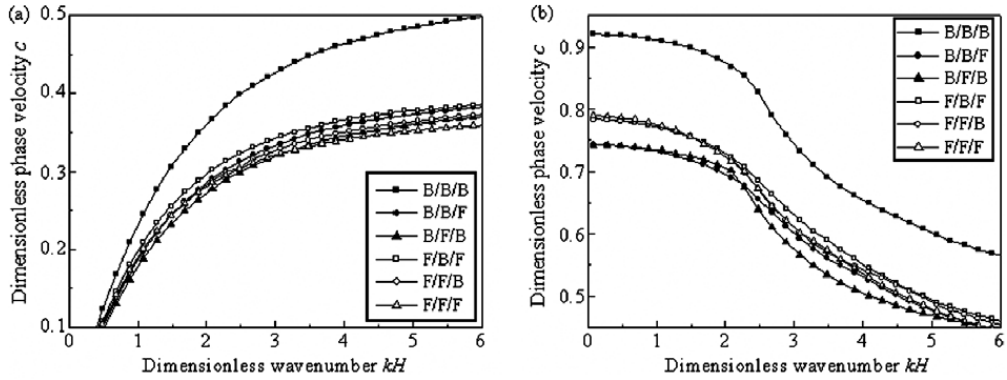

Fig. 5. Comparison of dispersion curves for the three-layered plates with different stacking sequences: (a) mode 1 and (b) mode 3.

Fig. 5(a) and (b) for modes 1 and 3, respectively. It is clear from Fig. 5(a) and (b) that the phase velocity corresponding to the B only (i.e., the B/B/B stacking sequence) is much larger than those corresponding to the other stacking sequences. This sharp difference in the dispersion curves for different stacking sequences is perhaps due to the fact that the maximum elastic stiffness element for $BaTiO_3$ is smaller than that in $CoFe_2O_4$ whilst both have nearly the same mass density. We also observe that the dispersion curves corresponding to the other stacking sequences (except for the B only) are all very close to each other, and that for those on mode 3 (Fig. 5(b)) they are apparently separated into two groups: Group 1 (with two B layers) consists of B/B/F and B/F/B, and Group 2 (with one B layer or F only) consists of F/B/F, F/F/B, and F only. Another interesting feature associated with Fig. 5(b) is that, for small wavenumber, the phase velocity in Group 1 is smaller than that in Group 2.

In order to analyze the dispersion feature in more detail, we have also studied the modal shapes associated with different modes at given wavenumbers. First, listed in Table 3 are some of the low natural frequencies for the six stacking sequences at wavenumber $kH = 2$. The natural frequencies are normalized as

Table 3
Dimensionless natural frequencies Ω at $kH = 2$

Stacking sequences	Mode				
	1	2	3	4	5
B only	0.7224	1.0355	1.7471	1.9049	2.5497
F only	0.5614	0.8889	1.4462	1.5341	1.9824
B/F/B	0.5453	0.8349	1.4105	1.4741	1.9174
F/B/F	0.5943	0.8817	1.4564	1.5798	2.1196
B/B/F	0.5710	0.8324	1.3906	1.5171	2.0316
F/F/B	0.5655	0.8790	1.4567	1.5415	1.9965

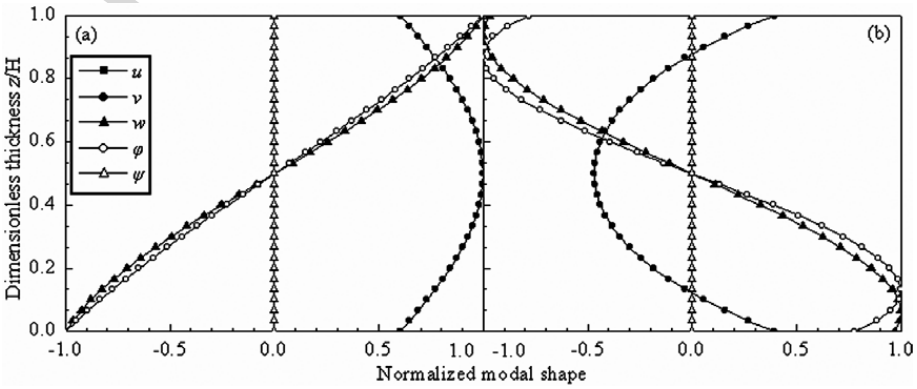

Fig. 6. Third modal shapes in B only (B/B/B) plate: (a) $kH = 2$ and (b) $kH = 5$.

$\Omega = \omega H/\sqrt{c_{\max}/\rho_{\max}}$. From Table 3, we notice that, on the same mode, the B/B/B (B only) stacking sequence has a high natural frequency as compared to those corresponding to the other stacking sequences where their frequencies are relatively close to each other. This actually also explains the dispersion feature we observed from Fig. 5 where the B/B/B stacking sequence has a larger phase velocity as compared to other sequences.

The third modal shapes for the general displacements (elastic displacement, and electric and magnetic potentials) in the thickness direction of the plate are presented in Figs. 6–11, with those corresponding to wavenumber $kH = 2$ in (a) and $kH = 5$ in (b). *First*, due to the material symmetry of transverse isotropy, the two horizontal displacement components (u and v) are the same on the same mode, and therefore their corresponding modal shapes overlap to each other in Figs. 6–11. *Second*, it is interesting that, for different

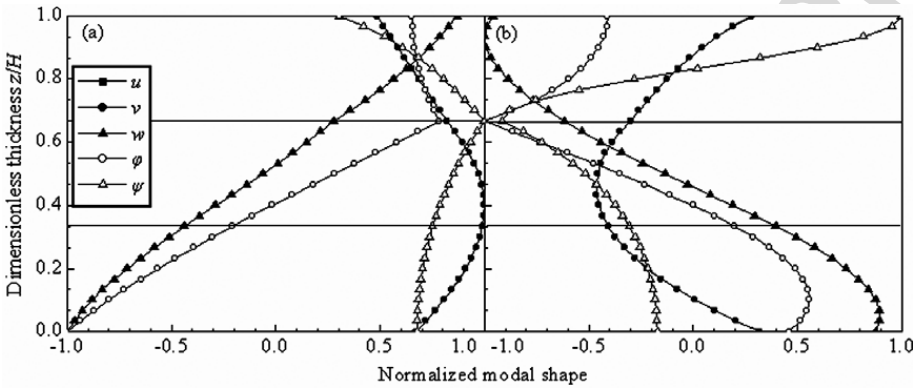

Fig. 7. Third modal shapes in B/B/F plate: (a) $kH = 2$ and (b) $kH = 5$.

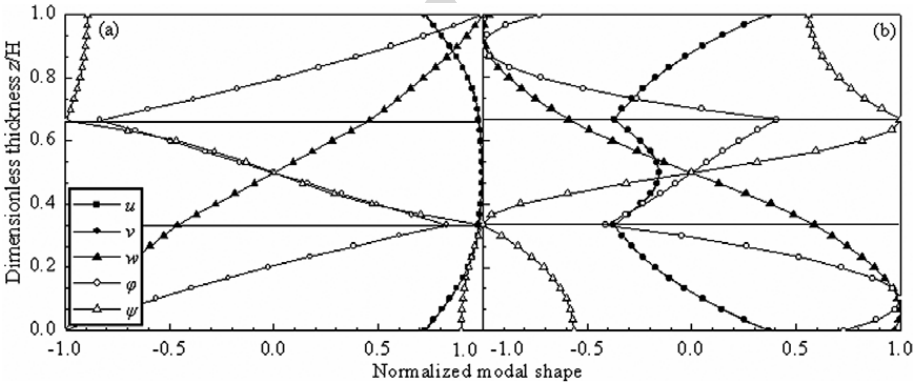

Fig. 8. Third modal shapes in B/F/B plate: (a) $kH = 2$ and (b) $kH = 5$.

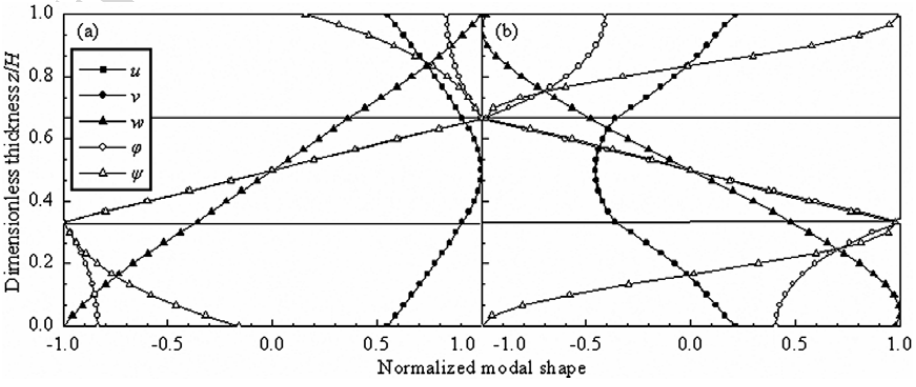

Fig. 9. Third modal shapes in F/B/F plate: (a) $kH = 2$ and (b) $kH = 5$.

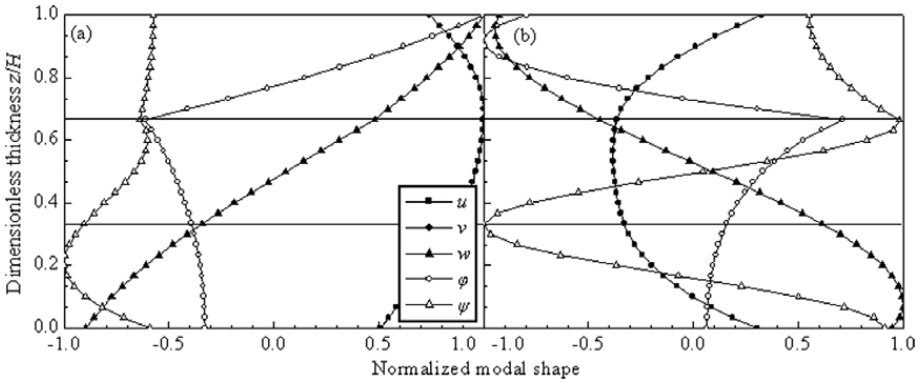

Fig. 10. Third modal shapes in F/F/B plate: (a) $kH = 2$ and (b) $kH = 5$.

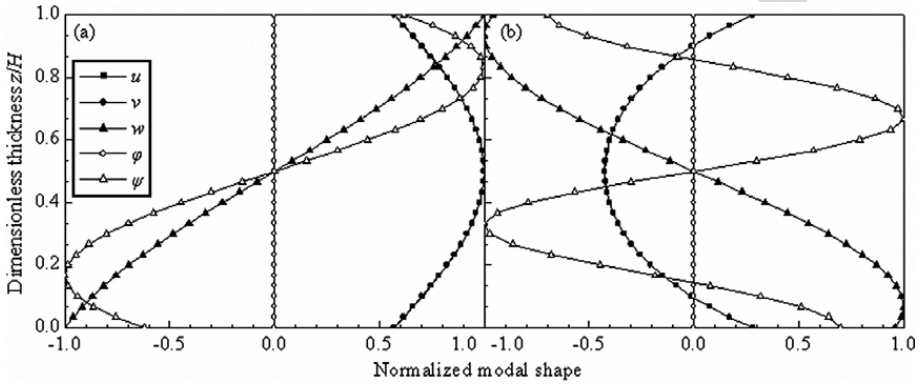

Fig. 11. Third modal shapes in F only (F/F/F) plate: (a) $kH = 2$ and (b) $kH = 5$.

stacking sequences, while the dispersion curves are very similar to each other (Figs. 4 and 5), their corresponding modal shapes are completely different (Figs. 6–11). *Third*, these modal shapes are exactly the same as those corresponding to the free vibration of the same layered plates but finite in lateral directions with simply supported conditions (Pan and Heyliger, 2002; Chen et al., in press). *Fourth*, for the given stacking sequence, the displacement modal shapes on $kH = 5$ (Figs. 6(b)–11(b)) are more complicated than those on $kH = 2$ (Figs. 6(a)–11(a)). *Fifth*, while the elastic displacement modal shapes are always smooth for different stacking sequences, with the except for the B/F/B plate with $kH = 5$ (Fig. 8(b)), the slope of the electric and magnetic potentials experience a discontinuity across the material interface (say from B to F), a clear correlation with the stacking sequence. *Finally*, for the B/B/F and F/F/B stacking sequences where the material property is not symmetric about the middle plane of the plate, the modal shapes are no longer symmetric (or anti-symmetric) about the middle plane, as shown in Figs. 7 and 10.

5. Conclusions

In this paper, the dispersion relation of the three-dimensional, anisotropic, magneto-electro-elastic, and multilayered plates has been derived. The state-vector approach and the propagator matrix method are introduced to solve the problem. The purely elastic and piezoelectric multilayered plates are first selected to verify the formulation proposed. Then typical numerical examples for the dispersion curves and modal shapes are presented for the piezoelectric and magnetic plates with six different stacking sequences (B/B/B, F/F/F, B/F/B, F/B/F, F/F/B, and B/B/F), including also the sandwich plates made of piezoelectric orthotropic materials. For the sandwich orthotropic plate, we found that the dispersion curve corresponding to the third mode is sensitive to the incident angle. For the sandwich plates made of piezoelectric and piezomagnetic materials, we observed that while the dispersion curves corresponding to different stacking sequences are only slightly different, the corresponding modal shapes can be remarkably different. We also noticed that the modal shapes

predicted in this paper are similar to those from the free vibration analysis. We finally calculated some of the low natural frequencies for the sandwich plate made of piezoelectric and piezomagnetic materials, and noticed that on the same mode the frequency for the B only plate is larger than those corresponding to the other stacking sequences.

Acknowledgements

This project was supported by the National Natural Science Foundation of PR China under Grant No. 50575172. The second author was also partially supported by ARO, AFOSR, and ODOT. The authors would like to thank the reviewers and the editor for their constructive comments, which are very helpful in revising the manuscript.

References

Achenbach, J.D., 1973. Wave Propagation in Elastic Solids. North-Holland, Amsterdam.
Achenbach, J.D., 2000. Quantitative nondestructive evaluation. International Journal of Solids and Structures 37, 13–27.
Bahar, L.Y., 1975. A state space approach to elasticity. Journal of Franklin Institute 229, 33–41.
Buchanan, G.R., 2003. Comparison of effective moduli for multiphase magneto-electro-elastic materials. In: Proceedings of the Tenth International Conference on Composite/Nano Engineering, New Orleans.
Chen, W.Q., Lee, K.Y., Ding, H.J., 2005. On free vibration of non-homogeneous transversely isotropic magneto-electro-elastic plates. Journal of Sound and Vibration 279, 237–251.
Chen, J.Y., Chen, H.L., Pan, E., Heyliger, P.R., in press. Modal analysis of magneto-electro-elastic plates using the state-vector approach. Journal of Sound and Vibration.
Chen, Z.R., Yu, S.W., Meng, L., Lin, Y., 2002. Effective properties of layered magneto-electro-elastic composites. Composite Structures 57, 177–182.
Chimenti, D.E., 1997. Guided waves in plates and their use in material characterization. Applied Mechanics Reviews 50, 247–284.
Fahmy, A.H., Adler, E.L., 1973. Propagation of acoustic surface waves in multilayer: a matrix description. Applied Physics Letters 22, 495–497.
Faidi, W.I., Nayfeh, A.H., 2000. An improved model for wave propagation in laminated piezoelectric composites. Mechanics of Materials 32, 235–241.
Gilbert, F., Backus, G., 1966. Propagator matrices in elastic wave and vibration problems. Geophysics 31, 326–332.
Graff, K.F., 1975. Wave Motion in Elastic Solids. Ohio State University Press, Ohio, USA.
Haskell, N.A., 1953. The dispersion of surface waves on a multilayered media. Bulletin of the Seismological Society of America 43, 17–34.
Jones, J.P., 1964. Wave propagation in a two-layered medium. Journal of Applied Mechanics 31, 213–222.
Karunasena, W.M., Shah, A.H., Datta, S.K., 1991. Reflection of plane strain waves at the free edge of a laminated composite plate. International Journal of Solids and Structures 27, 949–964.
Lee, J.S., Jiang, L.Z., 1996. Exact electroelastic analysis of piezoelectric laminate via state space approach. International Journal of Solids and Structures 33, 977–990.
Liu, H., Wang, Z.K., Wang, T.J., 2001. Effect of initial stress on the propagation behavior of Love waves in a layered piezoelectric structure. International Journal of Solids and Structures 38, 37–51.
Liu, G.R., Dai, K.Y., Han, X., Ohyoshi, T., 2003. Dispersion of waves and characteristic wave surfaces in functionally graded piezoelectric plates. Journal of Sound and Vibration 268, 131–147.
Minagawa, S., 1995. Propagation of harmonic waves in a layered elasto-piezoelectric composite. Mechanics of Materials 19, 165–170.
Pan, E., 1997. Static Green's functions in multilayered half-spaces. Applied Mathematical Modelling 21, 509–521.
Pan, E., 2001. Exact solution for simply supported and multilayered magneto-electro-elastic plates. Journal of Applied Mechanics 68, 608–618.
Pan, E., Heyliger, P.R., 2002. Free vibrations of simply supported and multilayered magneto-elector-elastic plates. Journal of Sound and Vibration 252, 429–442.
Pan, E., Rogers, J., Datta, S.K., Shah, A.H., 1999. Mode selection of guided waves for ultrasonic inspection of gas pipelines with thick coating. Mechanics of Materials 31, 165–174.
Ramirez, F., Heyliger, P.R., Pan, E., 2006. Free vibration response of two-dimensional magneto-electro-elastic laminated plates. Journal of Sound and Vibration 292, 626–644.
Safaeinili, A., Chimenti, D.E., Auld, B.A., Datta, S.K., 1995. Floquet analysis of guided waves propagating in periodically layered composites. Composites Engineering 5, 1471–1476.
Shin, K.H., Inoue, M., Arai, K.I., 1998. Preparation and properties of elastically coupled electro-magnetic elements with a bonding structure. IEEE Transactions on Magnetics 34, 1324–1326.
Stewart, J.T., Yong, Y.K., 1994. Exact analysis of the propagation of acoustic waves in multilayered anisotropic piezoelectric plates. IEEE Transactions on Ultrasonics, Ferroelectrics, and Frequency Control 41, 375–390.
Thomson, W.T., 1950. Transmission of elastic waves through a stratified medium. Journal of Applied Physics 21, 89–93.

Wang, L., Rokhlin, S.I., 2002. Recursive asymptotic stiffness matrix method for analysis of surface acoustic wave devices on layered piezoelectric media. Applied Physics Letters 81, 4049–4051.

Wang, Z., Rokhlin, S.I., 2004. A compliance/stiffness matrix formulation of general Green's function and effective permittivity for piezoelectric multilayers. IEEE Ultrasonics, Ferroelectrics, and Frequency Control 51, 453–463.

Wang, J.G., Chen, L.F., Fang, S.S., 2003. State vector approach to analysis of multilayered magneto-electro-elastic plates. International Journal of Solids and Structures 40, 1669–1680.

Wang, Q., Varadan, V.K., 2002. Wave propagation in piezoelectric coupled plates by use of interdigital transducer. Part 1. Dispersion characteristics. International Journal of Solids and Structures 39, 1119–1130.